Supporting Information (SI):

Experimental and DFT Investigation on Adsorption-Regeneration Performance and Deactivation Mechanism over Engineered Carbon Fiber: Role of Pore Structure and Functional Groups

Weiping Zhang,[a,b] Xiaoqin Wang,[a,b] Haiyong Pan,[a,b] Xingye Zeng, [c] Guiying Li,[a,b] Hongli Liu,[a,b] Jiejing Kong,[a,b] Huijun Zhao,[d] and Taicheng An *[a,b]

[a] *Guangdong Key Laboratory of Environmental Catalysis and Health Risk Control, Guangdong Hong Kong-Macao Joint Laboratory for Contaminants Exposure and Health, Institute of Environmental Health and Pollution Control, Guangdong University of Technology, Guangzhou 510006, China*

[b] *Guangdong Engineering Technology Research Center for Photocatalytic Technology Integration and Equipment, Guangzhou Key Laboratory of Environmental Catalysis and Pollution Control, School of Environmental Science and Engineering, Guangdong University of Technology, Guangzhou 510006, China*

[c] *Key Laboratory of Inferior Crude Oil Processing of Guangdong Provincial Higher Education Institutes, Guangdong University of Petrochemical Technology, Maoming 525000, P. R. China*

[d] *Centre for Clean Environment and Energy, Gold Coast Campus, Griffith University, Queensland 4222, Australia*

Corresponding Author: Prof. Taicheng An, E-mail: antc99@gdut.edu.cn

Table of contents

Experiments: Materials, Boehm Titration Experiment, Chemosorption and Desorption Test, Theoretical Calculation, In Situ DRIFTS, Byproducts Analysis.

Experiments

Materials:

Bacterial cellulose was purchased from Guilin Qihong Technology Store (Guangxi, China). Hydrochloric acid (HCl＞98.0%), sodium hydroxide (NaOH), sodium bicarbonate (NaHCO$_3$, 99%), sodium carbonate (Na$_2$CO$_3$, 99%), and methyl alcohol (MeOH) were provided by Guangzhou Weigu Technology Co., Ltd (Guangzhou, China). Methyl red, Bromocresol green, Potassium hydrogen phthalate, ethanol (C$_2$H$_6$O, 95%) and phenolphthalein were obtained from Macklin Biochemical Co., Ltd. All of the chemical reagents were analytical-grade and used as received without further purification. Deionized water was used throughout the experiments.

Boehm Titration Experiment:

The adsorbents possessed oxygen functionalities in the form of carboxylic, lactonic, phenolic and basic groups, which could be quantitatively determined via the so-called acid–base neutralization method of Boehm titration [1, 2]. To ensure titration precision, back-titration were adopted to reduce the impact of CO$_2$. For each analysis, 70 mg of adsorbents were added to 30 mL of 0.05 M NaHCO$_3$, NaOH, HCl and 15 mL of 0.05 M Na$_2$CO$_3$ solution, respectively. The solutions were agitated for 24 h and then filtered and collected the filtrates. The filtrates were acidified with excessive 0.05 M HCl. Then, the acidified solutions were purged with nitrogen to expel CO$_2$. The purge time was set from 120 to 180 min. After CO$_2$ expulsion, the solution was back-titrated with 0.05 M NaOH. A color indicator of phenolphthalein was used for endpoint determination. For each adsorbent and reaction base, samples were tested in triplicate with a parallel blank reference. During titration, the blank sample was exposed to the same procedures that were applied to adsorbents samples. The final result was calculated with the averaged measurement minus the blank.

EA-TPD Test:

The temperature programmed desorption (TPD) experiment of ethyl acetate (EA) from porous carbon adsorbents was conducted at different ramping rates of temperature [3]. In each measurement, precisely weighted 30 mg adsorbent was first pretreated in a purge of Ar at

150 °C for 1 h. After being cooled to room temperature under flowing Ar, the sample was exposed to a mixture gas containing 200 ppm EA for 60 min, and then purged with Ar for 1 h to remove physiosorbed ethyl acetate. Finally, the EA-TPD profiles were measured as a function of temperature from 303 to 800 K with various heating rate from 3 to 10 K min^{-1} under Ar flow (30 mL min^{-1}). The desorption activation energies (E_d) of EA on the CBC adsorbent samples could be calculated based on their TPD curves. The expression for the E_d was calculated based on the Polanyi–Wigner Eq S1:

$$-\ln\left(\frac{\beta_H}{RT_p^2}\right) = \frac{E_d}{RT_p} + ln\square(\frac{E_d}{k_0})$$

where Ed (kJ•mol^{-1}) represents the desorption activation energy of EA on the adsorbate, β_H (K•min^{-1}) refers to the heating rate, and T_p (K) refers to the temperature of the peak in the desorption curve.

Regeneration Test:

In addition, the regeneration experiments were carried out by hot nitrogen gas purge. After the adsorbent reached adsorption equilibrium, the inlet gas was switched to N_2 with a flow rate of 30 mL min^{-1}. The regeneration temperature was 120 ℃, and the regeneration time was 6 h. Then, the adsorbent was cooled to room temperature and reused in the next adsorption cycle. The adsorption/desorption experiments were carried out for four cycles.

Theoretical Calculation:

The adsorption behavior of the EA molecule adsorbed on CBC surfaces were investigated with the DMol3 program package based on the density functional theory (DFT) calculations and aperiodic finite plane method. Considering the complexity and uncertainty of activated carbon structure, a graphene cluster models with coronene-shaped basis unit structure was chosen as the carbon model for quantum chemistry calculations [4-6]. And the model of carbonaceous materials consists of 66 C atoms, 22 terminating H atoms and 23 aromatic rings with no branch. Moreover, functionalized carbon sheets were modeled by substituting C atom with O atom based on the functional groups. The adsorption energy E_{ads} between the EA and surface model was calculation in the following manner:

$$E_{ads} = E_{surface+EA} - (E_{surface} + E_{EA}) \qquad (1)$$

where $E_{surface}$, E_{EA} and $E_{surface+EA}$ are the energy of the substrate surface, the energy of the isolated EA molecule and the total energy of the adsorbate–substrate system, respectively. Three configurations for the EA adsorption on the surface models were considered to compare the effect of different adsorption direction on EA adsorption: (A) parallel to the adsorbed surface, and therefore, three initial adsorption systems have been fully optimization; (B) perpendicular to the surface, O atom near the adsorbed surface; (C) perpendicular to the surface, H atom near to the adsorbed surface.

In Situ DRIFTS:

In situ DRIFTS experiment refer to our previously published literature[7]. Ethyl acetate adsorption on the synthesized adsorbents were recorded on a Thermo Scientific Nicolet iS10 Fourier transform infrared spectrometer equipped with a MCT detector. Prior to each adsorption test, the adsorbent was loaded into a porous screen at the bottom of a Harrick Scientific Praying Mantis diffuse reflectance cell which had two ZnSe windows and one glass observation window and then the cell was sealed with a dome. After 20 min of nitrogen purging to remove the gas from the adsorption chamber, the sample was heated to 150 °C in a 30 mL min^{-1} N$_2$ flow for 120 min. After cooling to 30 °C, a background spectrum of the adsorbent was firstly obtained in the N$_2$ flow, followed by switching N$_2$ to ethyl acetate stream (30 mL min^{-1}) for the adsorption experiment. The signals of infrared information on the adsorbents surface were collected every 10 min for a total of 50 minutes. All DRIFT spectra were recorded at a resolution of 4 cm^{-1} in the range of 4000 to 400 cm^{-1}.

Byproducts Analysis:

After various adsorption-desorption cycling, the intermediates were separated and extracted as following steps[8]. 0.02 g of adsorbed after the adsorption-desorption cycling was transferred into a 100 mL of conical flask with 60 mL methanol (Shanghai ANPEL Laboratory Technologies Inc.) and disposed under ultrasonic condition for 30 min. The obtained suspension was filtered, and the mixed extract was concentrated to 1 mL by a rotary evaporator, averaged into two 1.5 mL vials, and then completely dried with a gentle stream of high-purity nitrogen. For direct detection of intermediates, one portion of the sample was re-dissolved in 0.75 mL EA (Shanghai ANPEL Laboratory Technologies Inc.) and then injected

into the gas chromatograph (Agilent 7890B) coupled with a mass selective detector (Agilent 5977B) (GC–MSD) with a HP-5ms column (30 m × 0.25 mm × 0.25 μm film thickness). Another portion was derived overnight at 25 °C using 50 μL N, O-bis-(trimethylsilyl)-trifluoroacetamide (BSTFA) as derivation reagent for GC–MS detection. Temperature program of column was 60 °C for 1 min, rose to 161 °C at 5 °C min^{-1} holding for 1 min and rose to 280 °C at 10 °C min^{-1} holding for 3min. Mass spectra were recorded in electron ionization mode at an ion source temperature of 230 °C.
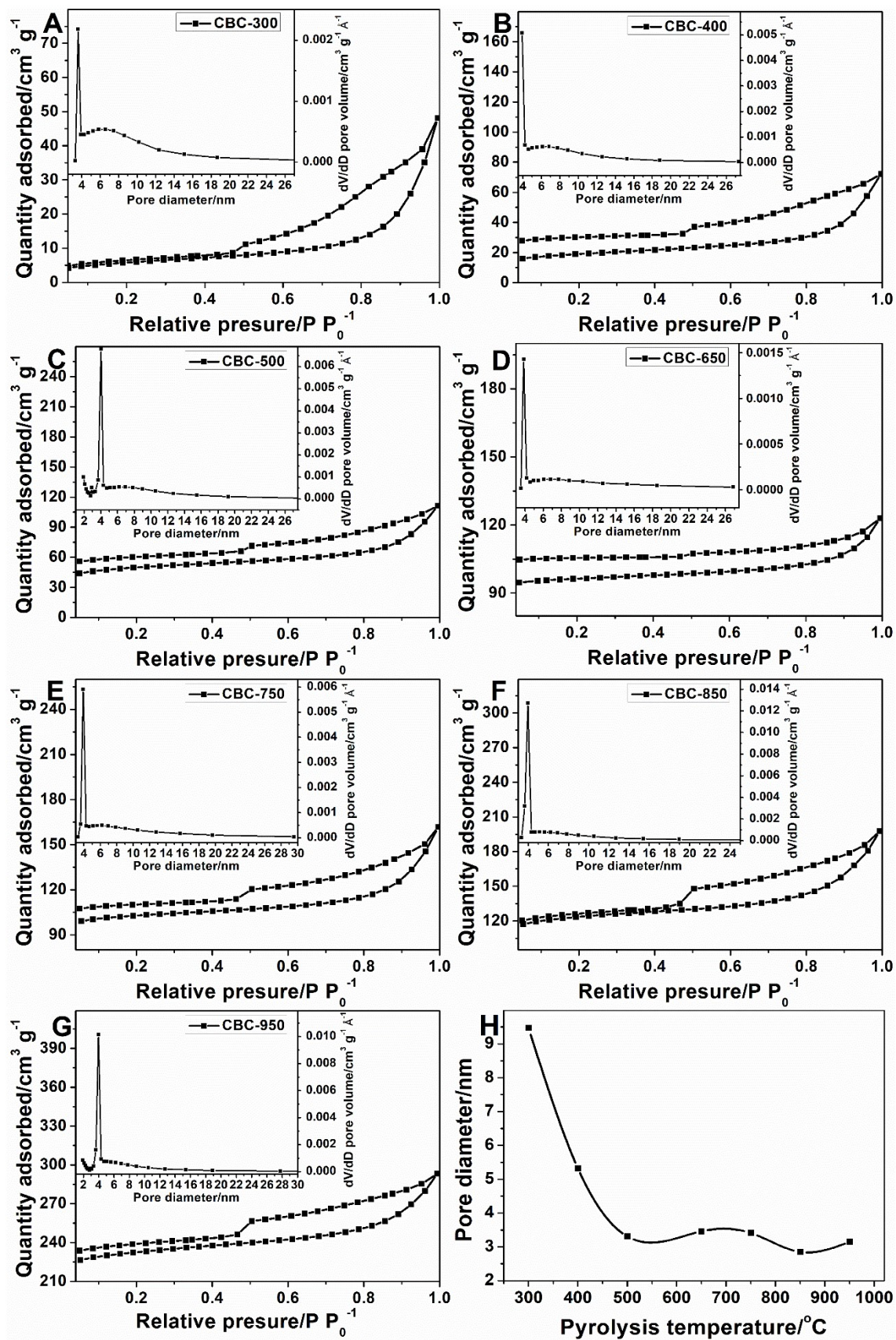
Fig. S1. N_2 adsorption-desorption isotherms and pore distribution of CBC synthesized at different pyrolysis temperatures.

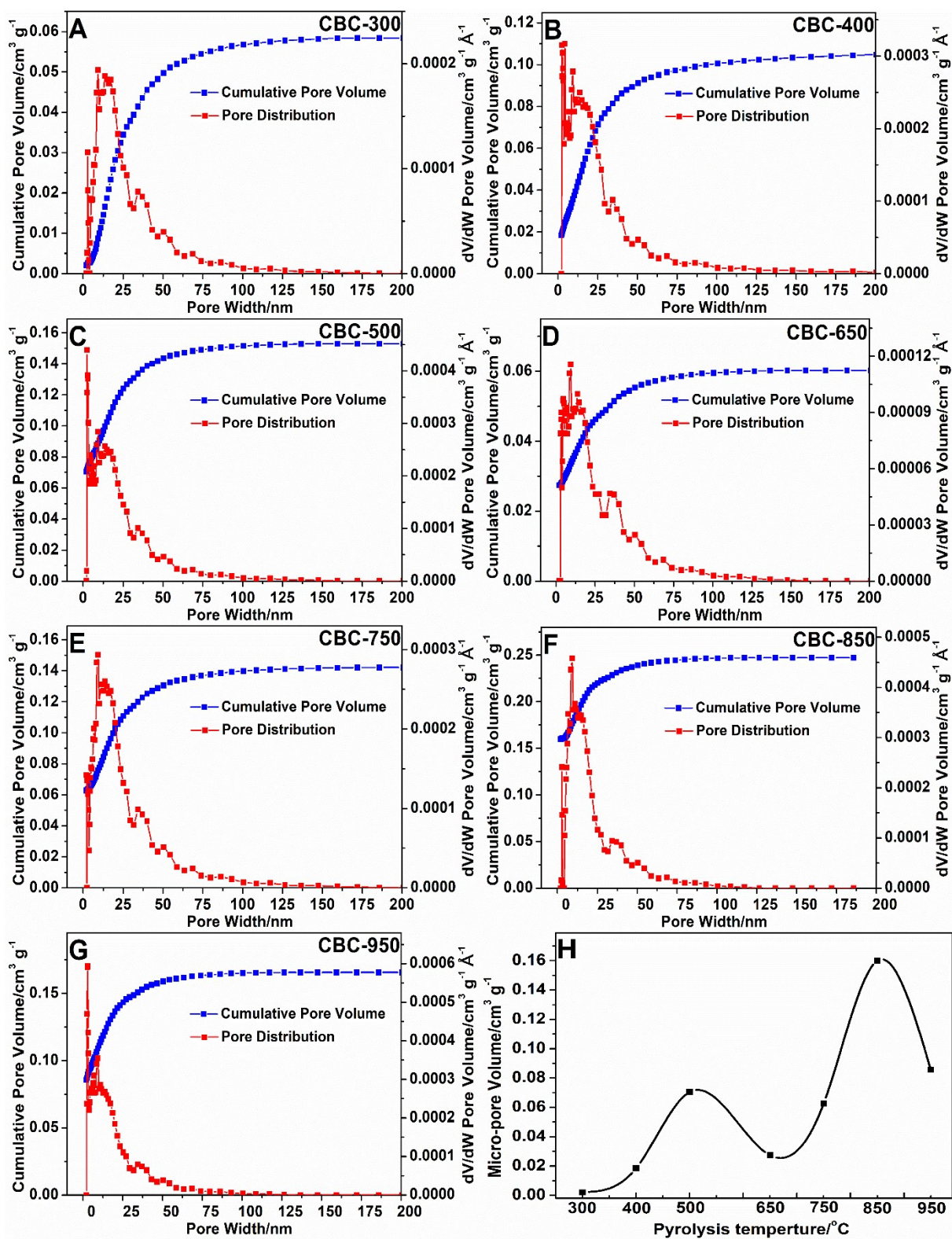**Fig. S2.** DFT pore distribution and cumulative pore volume (A, B, C, D, E, F and G) and micropore volume

(H) of CBC synthesized at different pyrolysis temperatures.
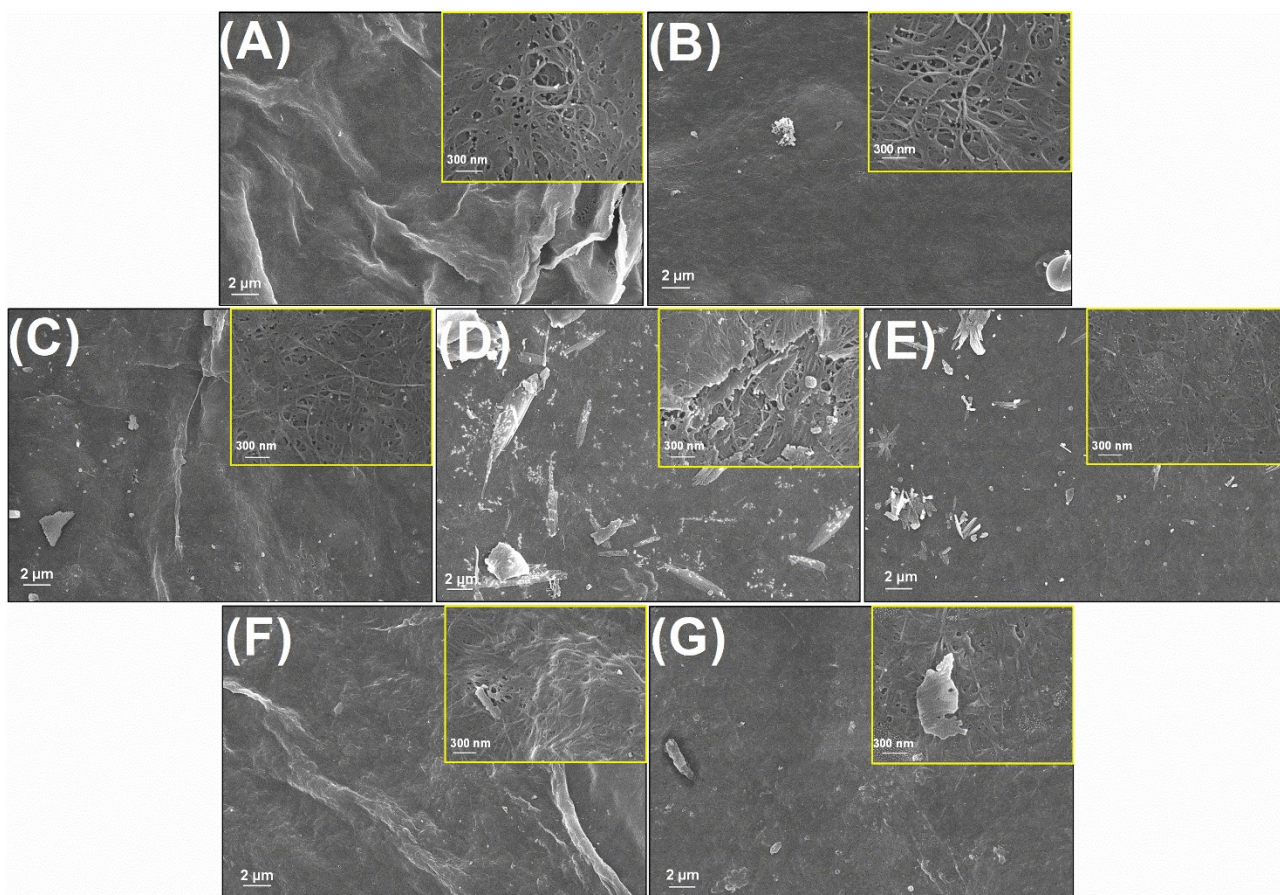
Fig. S3. SEM images of CBC adsorbents prepared at different pyrolysis temperatures: (A, CBC-300; B, CBC-400; C, CBC-500; D, CBC-650; E, CBC-750; F, CBC-850; G, CBC-950).
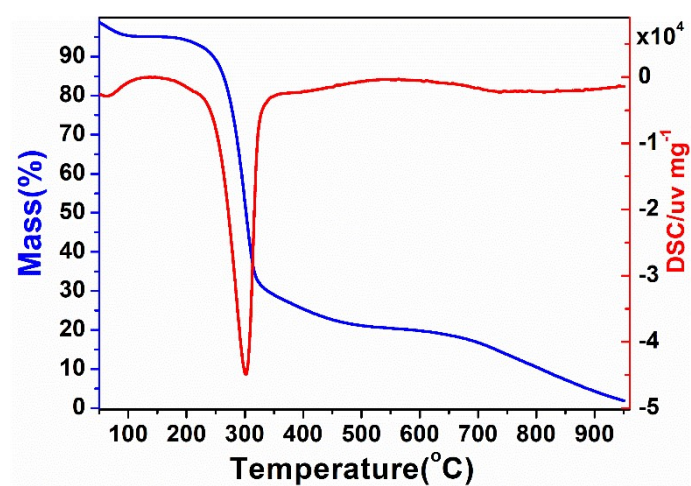

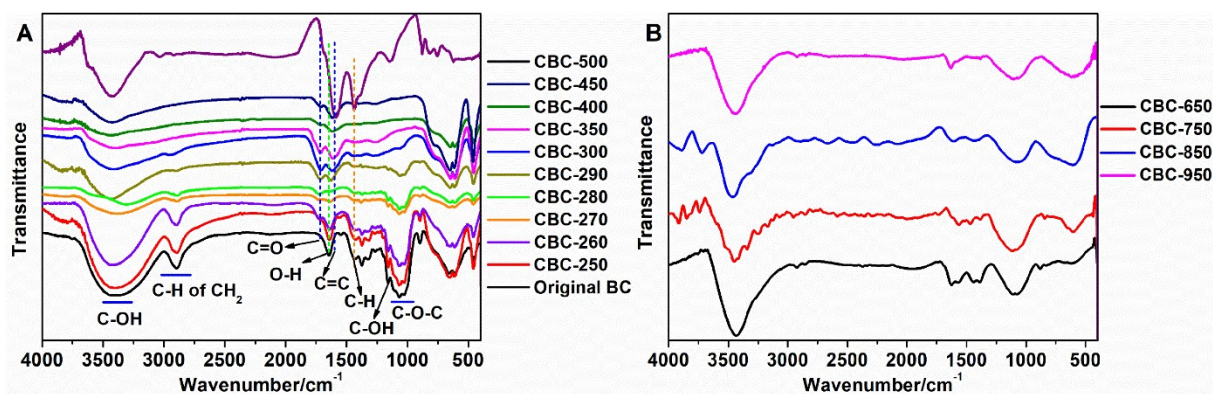**Fig. S4.** TG-DSC curves of BC pyrolyzed with argon gas protection.

Fig. S5. FT-IR spectra of CBC synthesized at different pyrolysis temperatures (A, low temperature; B, high temperature).

When the pyrolysis temperature gradually increased from 250 ℃ to 350 ℃, C-O or C-OH functional groups almost disappeared in the range of 940~1220 cm^{-1}, indicating the pyrolysis transformation of C-O bond on the adsorbent. Meanwhile, new peaks located at 1715 cm^{-1} and 1623 cm^{-1} were observed, corresponding to C=O and C=C of benzene ring structure respectively, which indicated that the pyrolysis process not only involved dehydration and condensation reaction but also promoted the formation of porous carbon with phenyl ring structure. When the pyrolysis temperature gradually rises from 330 ℃ to 650 ℃, the decrease of the peak value of carboxyl group expands, which is mainly a C=O drop process. With further increasing pyrolysis temperature, oxygen-containing functional groups almost disappeared.
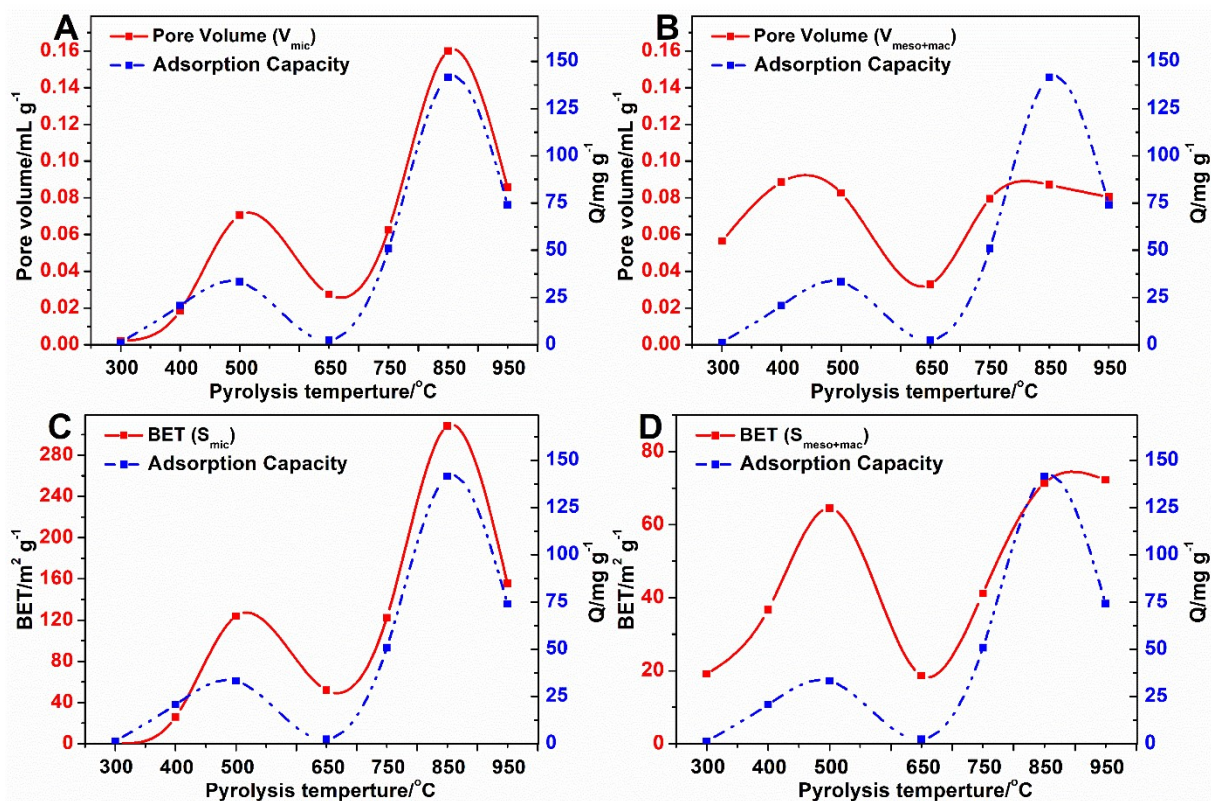
Fig. S6. The relationship between pore volume (A and B) and BET (C and D) and adsorption capacity of CBC synthesized at different pyrolysis temperatures.

Fig. S7. Desorption rate of CBC adsorbents synthesized at different pyrolysis temperatures.
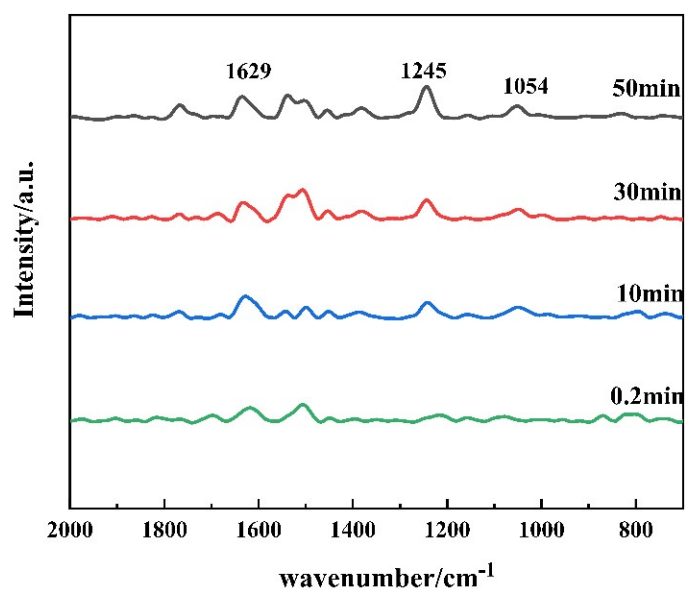
Fig. S8. Time-dependent in-situ DRIFTS of EA adsorption over CBC-950.
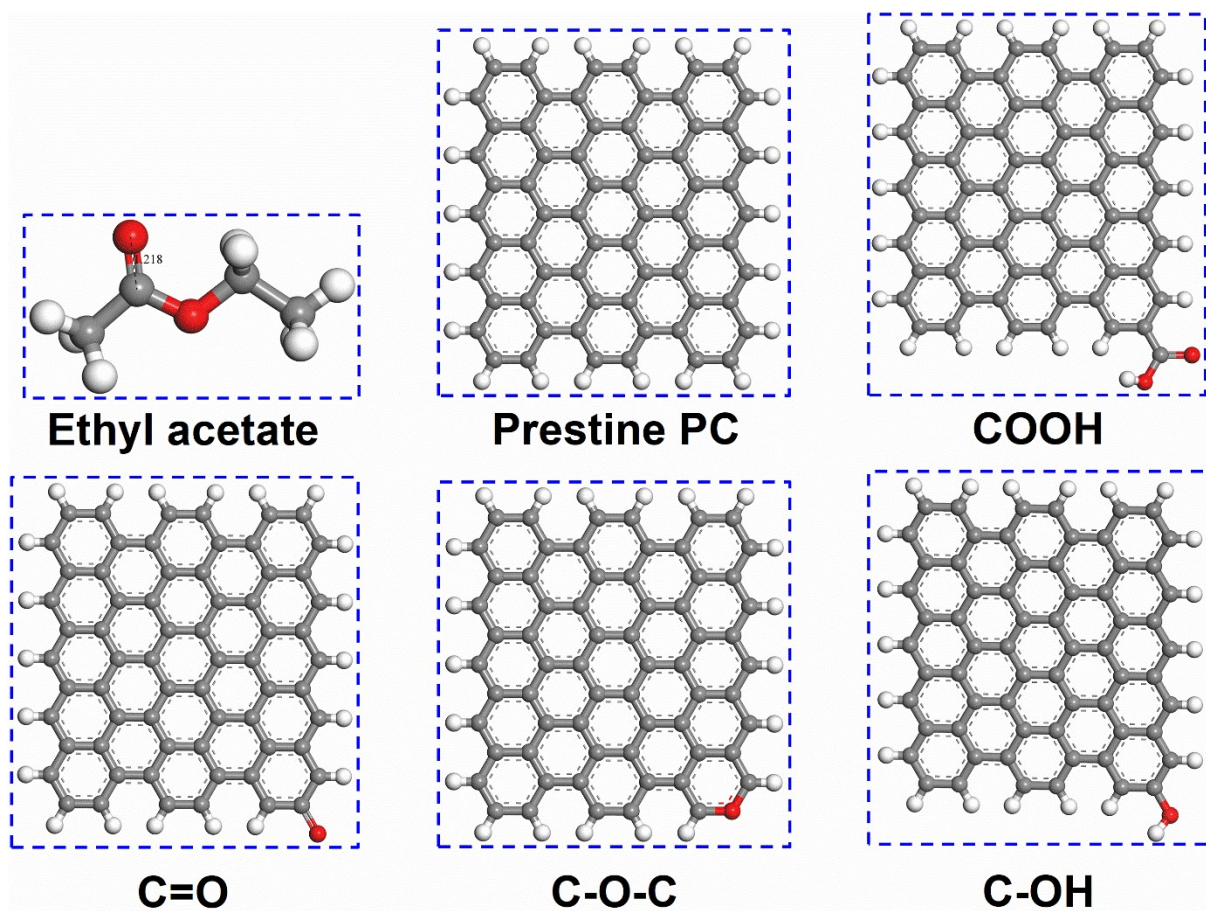
Fig. S9. Optimized structures of ethyl acetate molecule and surface model.
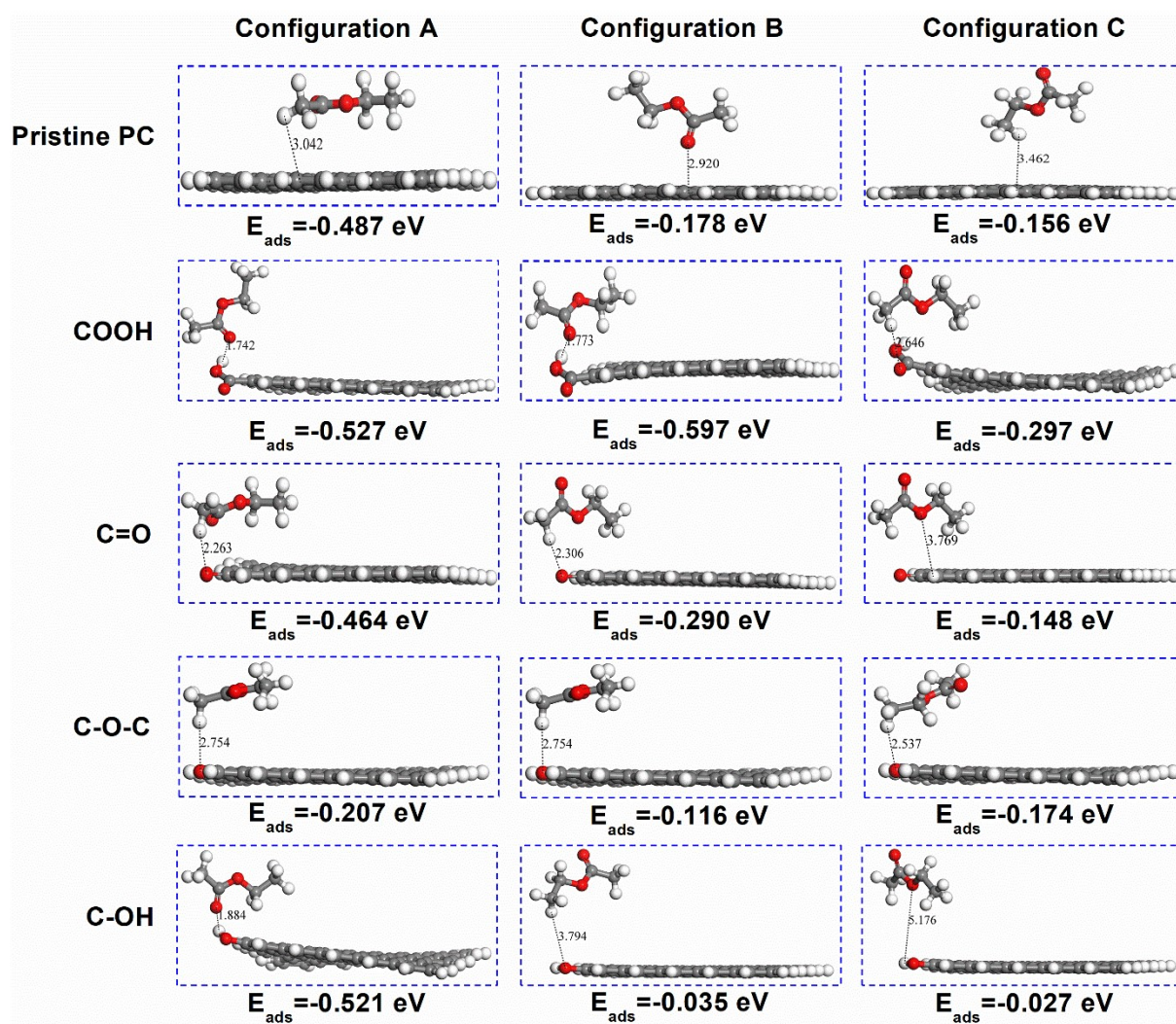
Fig. S10. Monolayer adsorption interaction of ethyl acetate with O-containing functional group surface.

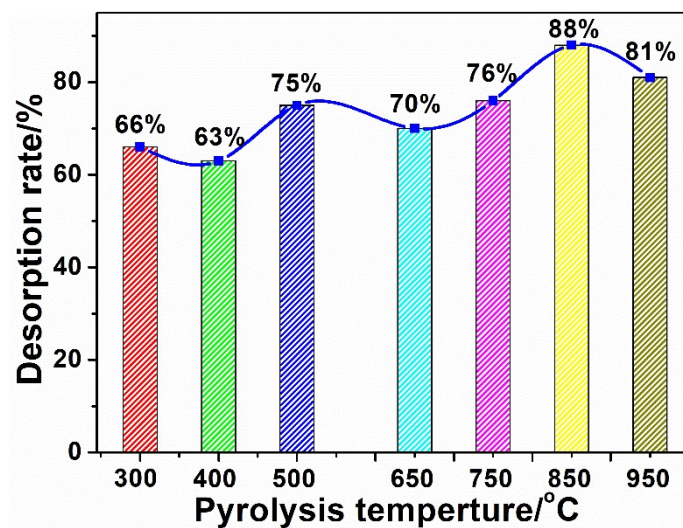|	Configuration A	Configuration B	Configuration C
Pristine PC	E_{ads}=-0.620 eV	E_{ads}=-0.099 eV	E_{ads}=-0.170 eV
COOH	E_{ads}=-0.735 eV	E_{ads}=-0.670 eV	E_{ads}=-0.654 eV
C=O	E_{ads}=-0.431 eV	E_{ads}=-0.392 eV	E_{ads}=-0.244 eV
C-O-C	E_{ads}=-0.256 eV	E_{ads}=-0.595 eV	E_{ads}=-0.345 eV
C-OH	E_{ads}=-0.743 eV	E_{ads}=-0.550 eV	E_{ads}=-0.390 eV

Fig. S11. Multilayer adsorption interaction of ethyl acetate with O-containing functional group surface.
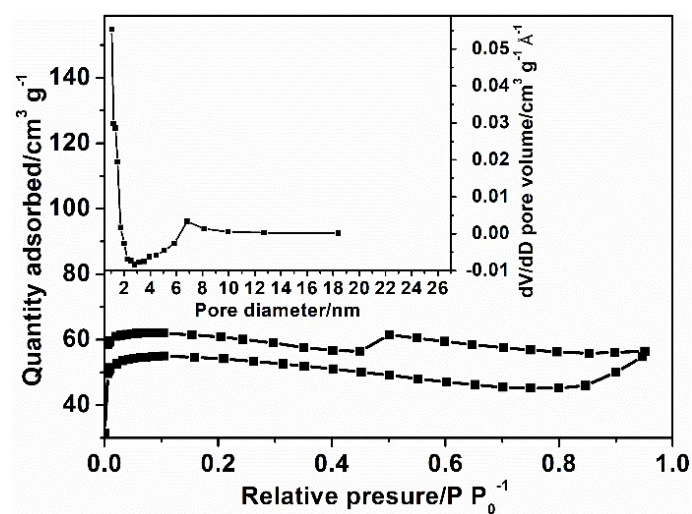
Fig. S12. N_2 adsorption-desorption isotherms and pore distribution of CBC-850 with six adsorption-desorption cycles.
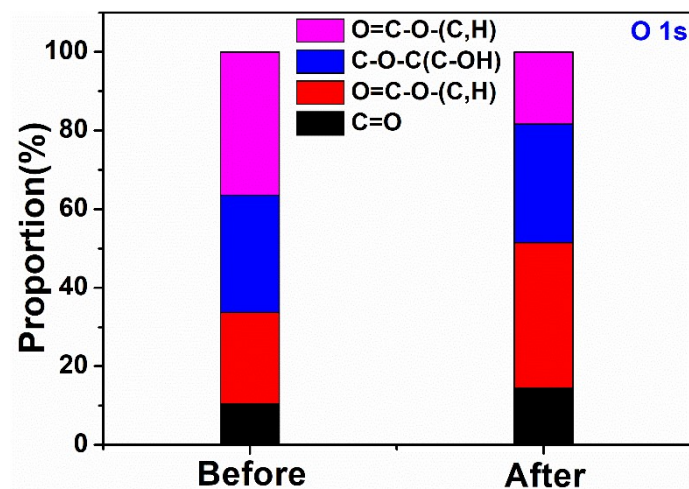
Fig. S13. Proportion of functional groups on CBC-850 by deconvolution of O1s spectra.

Table S1. Porous structure parameters of the tested CBC samples.

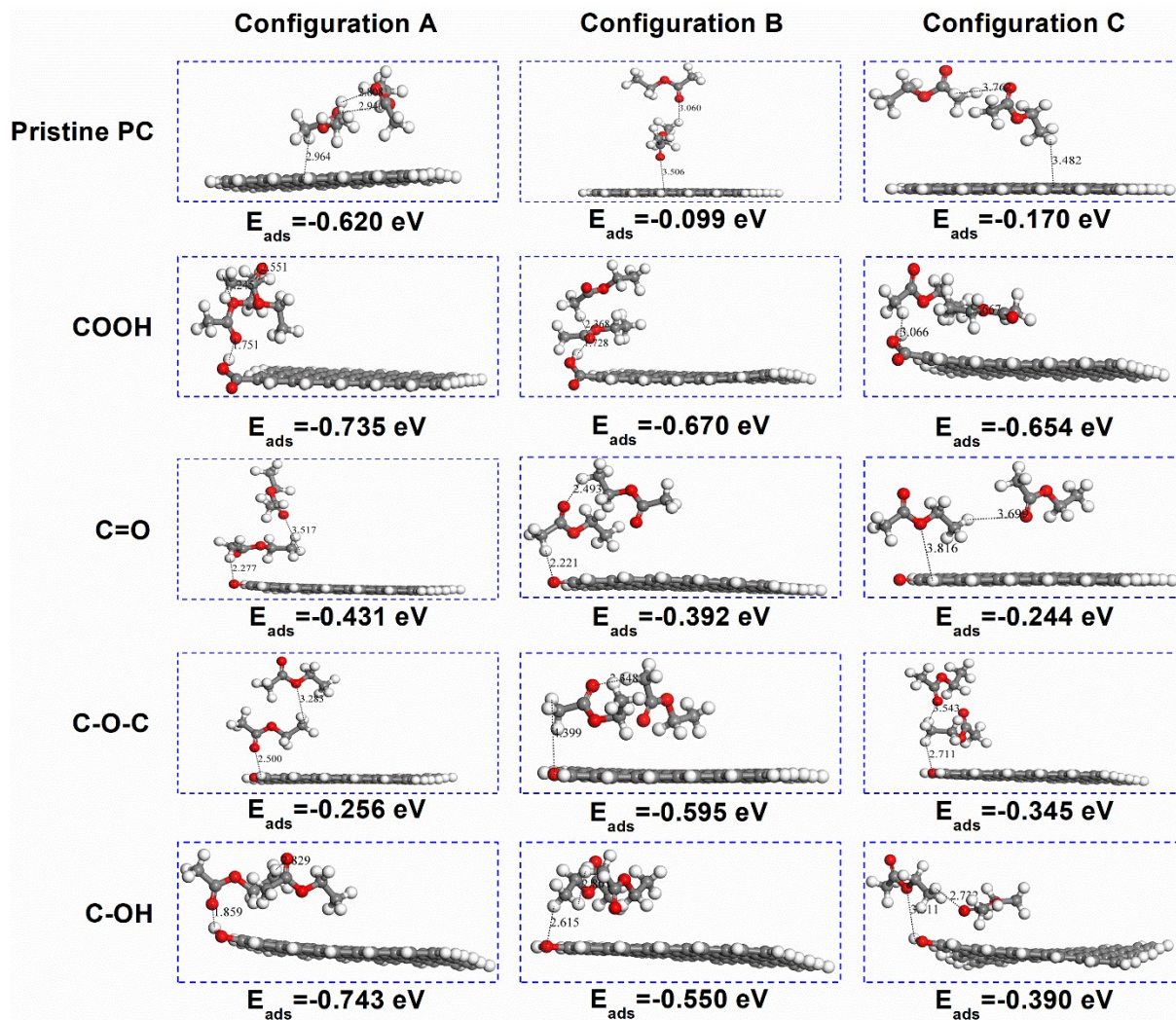| Sample name | D_{BET} (nm) | S_{BET} (m^2 g^{-1}) | S_{mic} (m^2 g^{-1}) | $S_{meso+Mac}$ (m^2 g^{-1}) | *Porosity Distribution by DFT Model* | | |
					V_{total} (mL g^{-1})	V_{mic} (mL g^{-1})	$V_{meso+Mac}$ (mL g^{-1})
CBC-300	9.47	20.42	1.30	19.12	0.0584	0.00211	0.0563
CBC-400	5.32	62.61	25.91	36.70	0.107	0.0185	0.0885
CBC-500	3.31	188.48	124.00	64.48	0.153	0.0705	0.0825
CBC-650	3.46	70.45	51.81	18.64	0.0603	0.0274	0.0329
CBC-750	3.41	163.66	122.43	41.23	0.142	0.0626	0.0794
CBC-850	2.85	379.70	308.40	71.30	0.247	0.160	0.087
CBC-950	3.15	227.64	155.42	72.22	0.166	0.0856	0.0804

Table S2. Concentration of oxygen-containing groups of CBC measured by a Boehm's titration quantitative method.

Samples	Concentration of oxygen-containing groups (μmmol g^{-1})			
	Carboxylic group	Phenolic group	Lactonic group	Basic group
CBC-300	1.443	2.579	2.525	1.235
CBC-400	0.729	2.289	2.475	1.414
CBC-500	0.612	2.015	2.029	1.867
CBC-650	0.364	1.088	2.500	0.319
CBC-750	0.329	0.834	0.225	1.485
CBC-850	0.0600	0.107	0.191	1.321
CBC-950	0.0400	0.00226	0.0850	1.323

Table S3. Spearman correlations of EA adsorption with pore structure and functional groups.

	T	Q	Carboxyl	Base	PhOH	Lactonyl	S_{BET}	S_{mic}	$S_{meso+Macro}$	V_{mic}	$V_{meso+Macr}$
T	1.000	0.857	-1.000	0.036	-1.000	-0.893	0.857	0.857	0.714	0.857	0.071
Q	0.857	1.000	-0.857	0.357	-0.857	-0.964	0.929	0.929	0.893	0.929	0.500
Carboxyl	-1.000	-0.857	1.000	-0.036	1.000	0.893	-0.857	-0.857	-0.714	-0.857	-0.071
Base	0.036	0.357	-0.036	1.000	-0.036	-0.393	0.250	0.250	0.464	0.250	0.536
PhOH	-1.000	-0.857	1.000	-0.036	1.000	0.893	-0.857	-0.857	-0.714	-0.857	-0.071
Lactonyl	-0.893	-0.964	0.893	-0.393	0.893	1.000	-0.893	-0.893	-0.929	-0.893	-0.429
S_{BET}	0.857	0.929	-0.857	0.250	-0.857	-0.893	1.000	1.000	0.857	1.000	0.357
S_{mic}	0.857	0.929	-0.857	0.250	-0.857	-0.893	1.000	1.000	0.857	1.000	0.357
$S_{meso+Macro}$	0.714	0.893	-0.714	0.464	-0.714	-0.929	0.857	0.857	1.000	0.857	0.536
V_{mic}	0.857	0.929	-0.857	0.250	-0.857	-0.893	1.000	1.000	0.857	1.000	0.357
$V_{meso+Macr}$	0.071	0.500	-0.071	0.536	-0.071	-0.429	0.357	0.357	0.536	0.357	1.000

Footnote: T=temperature/^{o}C; Q=adsorption capacity/mg g^{-1}; Concentration of functional group/μmmol g^{-1}; S/ m^2 g^{-1}; V/mL g^{-1}

Table S4. Desorption peak temperatures of EA at different heating rates and desorption activation

energies (Ed) of adsorbed-EA on CBC.

Samples	The peak temperature Tp (K) at different heating rates (K min^{-1})				Ed (kJ mol^{-1})
	3	5	7	10	
CBC-300	329	344	359	367	24.89
CBC-400	364	382	391	396	36.46
CBC-500	479	496	542	563	19.92
CBC-650	336	347	364	388	17.88
CBC-750	388	405	413	431	33.75
CBC-850	453	483	507	522	25.19
CBC-950	363	390	399	408	25.23

Table S5. Pore structure of CBC-850 before EA adsorption and after regeneration.

Sample name	D_{BET} (nm)	S_{BET} (m^2 g^{-1})	V_{total} (mL g^{-1})
CBC-850-Before	2.85	379.70	0.247
CBC-850-After	2.22	156.99	0.0873
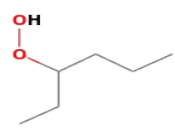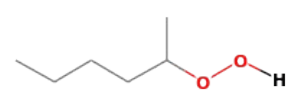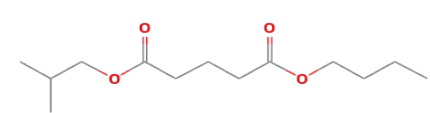
Table S6. Proportion of functional groups on CBC-850 by deconvolution of XPS C1s and O1s spectra.

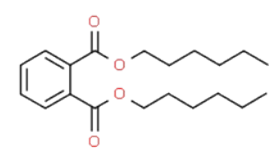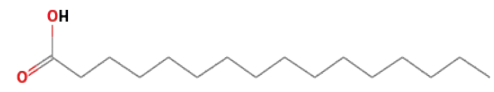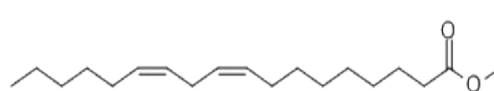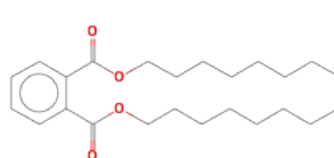|		CBC-850 before EA adsorption				CBC-850 after regeneration		
	Peak/ eV	Groups	Proportion/ %	Total /%	Peak/ eV	Groups	Proportion/ %	Total /%
C1s	284.8	C=C	68.47	91.28	284.8	C=C	63.68	84.58
	285.5	C-C	16.17		285.7	C-C	12.57	
	286.8	C-O	6.90		286.8	C-O	11.85	
	290.0	C=O	8.46		290.3	C=O	11.90	
O1s	530.9	C=O	10.52	8.72	531.2	C=O	14.61	15.42
	532.0	O=C-O-(C, H)	23.24		532.4	O=C-O-(C, H)	36.87	
	532.8	C-O-C (C-OH)	29.81		533.6	C-O-C (C-OH)	30.16	
	533.9	O=C-O-(C, H)	36.43		534.9	O=C-O-(C, H)	18.36	

Table S7. I_D/I_G and A_{sp3}/A_{sp2} of CBC adsorbents based on deconvolution of Raman spectra.

Sample name	I_D/I_G	A_{sp3}/A_{sp2}
CBC-850	2.701	0.599
CBC-850-regeneration	3.455	0.395

Table S8. Retention time, mass spectra and structure of the identified intermediates generated onto the surface of CBC-850 by GC-MSD during EA adsorption-desorption process.

Intermediates	Retention time (min)	Proposed structure
Hydroperoxide,1-ethylbutyl	3.974	
Hydroperoxide,1-methylpentyl	4.178	
Glutaric acid, butyl isobutyl ester	22.076	
1,2-Benzenedicarboxylic acid, dihexyl ester	27.267	
n-Hexadecanoic acid	30.211	
9, 12-octadecanoic acid methyl ester	33.809	
Dioctyl phthalate	39.865	

References:

1. H. P. Boehm, Surface oxides on carbon and their analysis: a critical assessment, *Carbon*, 2002, **40**, 145-149.
2. H. Wu, W. Lu, Y. Chen, P. Zhang and X. Cheng, Application of Boehm Titration for the Quantitative Measurement of Soot Oxygen Functional Groups, *Energ. Fuel.*, 2020, **34**, 7363-7372.
3. H. Liu, M. Xu, G. Li, W. Zhang and T. An, Solar-light-triggered regenerative adsorption removal of styrene by silver nanoparticles incorporated in metal–organic frameworks, *Environ. Sci-Nano*, 2021, **8**, 543-553.
4. K. Zhou, W. Ma, Z. Zeng, R. chen, X. Xu, B. Liu, H. Li, H. Li and L. Li, Waste biomass-derived oxygen and nitrogen co-doped porous carbon/MgO composites as superior acetone adsorbent: Experimental and DFT study on the adsorption behavior, *Chem. Eng. J.*, 2020, **387**, 124173.
5. G. Lim, K. B. Lee and H. C. Ham, Effect of N-Containing Functional Groups on CO2 Adsorption of Carbonaceous Materials: A Density Functional Theory Approach, *J. Phys. Chem. C,* 2016, **120**, 8087-8095.
6. F. Zheng, Y. Yang and Q. Chen, High lithium anodic performance of highly nitrogen-doped porous carbon prepared from a metal-organic framework, *Nat. Commun.*, 2014, **5**, 5261.
7. H. Liu, N. Li, M. Feng, G. Li, W. Zhang and T. An, Near-infrared light induced adsorption–desorption cycle for VOC recovery by integration of metal–organic frameworks with graphene oxide nanosheets, *Environ. Sci.: -Nano*, 2022, **9**, 1858-1868.
8. W. P. Zhang, G. Y. Li, H. L. Liu, J. Y. Chen, S. T. Ma, M. C. Wen, J. J. Kong and T. C. An, Photocatalytic degradation mechanism of gaseous styrene over Au/TiO$_2$@CNTs: Relevance of superficial state with deactivation mechanism, *Appl. Catal. B: Environ.*, 2020, **272**, 118969.